Temperature-tunable semiconductor metamaterial

K. L. Koshelev[1,2,*] and A. A. Bogdanov[1,2,3,†]
[1]*ITMO University, 197101 St. Petersburg, Russian Federation*
[2]*Ioffe Institute, 194021 St. Petersburg, Russian Federation*
[3]*Peter the Great St. Petersburg Polytechnic University, 195251 St. Petersburg, Russian Federation*
(Received 10 April 2015; revised manuscript received 19 July 2015; published 14 August 2015)

We propose a class of temperature-tunable semiconductor metamaterials for terahertz applications. These metamaterials are based on doped semiconductor superlattices with ultrathin barriers of about 1 nm thickness. Due to the tunnel transparency of the barriers, layers of the superlattice cannot be considered as isolated and, therefore, the classical homogenization approach is inapplicable. We develop a theory of quantum homogenization which is based on the Kubo formula for conductivity. The proposed approach takes into account the wave functions of the carriers, their distribution function, and energy spectrum. We show that the components of the dielectric tensor of the semiconductor metamaterial can be efficiently manipulated by external temperature and a topological transition from the dielectric to hyperbolic regime of metamaterial can be observed at room temperature. Using a GaAs/$Al_{0.3}Ga_{0.7}As$ superlattice slab as an example, we provide a numerical simulation of an experiment which shows that the topological transition can be observed in the reflectance spectrum from the slab.

DOI: 10.1103/PhysRevB.92.085305 PACS number(s): 78.67.Pt, 73.21.Cd, 73.21.Fg, 78.30.Fs

I. INTRODUCTION

Hyperbolic metamaterials (HMMs) are one of the fastest developing branches of modern optics [1–6]. The dielectric function of HMMs is described by a tensor with two different components corresponding to the directions along ($\varepsilon_\parallel$) and across ($\varepsilon_\perp$) the optical axis:

$$\varepsilon = \begin{pmatrix} \varepsilon_\perp & 0 & 0 \\ 0 & \varepsilon_\perp & 0 \\ 0 & 0 & \varepsilon_\parallel \end{pmatrix}. \quad (1)$$

Depending on the sign of these components, the crystal represents a dielectric medium ($\varepsilon_\perp > 0,\ \varepsilon_\parallel > 0$), a metal ($\varepsilon_\perp < 0,\ \varepsilon_\parallel < 0$), or a hyperbolic metamaterial ($\varepsilon_\perp \varepsilon_\parallel < 0$). For HMMs the shape of equal-frequency surface in **k** space represents a one- or two-sheet hyperboloid depending on the signature of permittivity tensor [5]. This results in a singularity of the photon density of states and explains the unique optical properties of HMMs [7].

In tunable metamaterials, the dielectric and magnetic responses and, therefore, the shape of equal-frequency surface can be manipulated by various external influences [8], for example, by temperature [9–11] or gate voltage [12]. In highly tunable metamaterials, the signature of the permittivity tensor can be switched, changing the equal-frequency surface topology. This phenomenon is called topological transition [9,13,14]. It has been experimentally observed in some systems [9,15].

Fabrication of tunable THz metamaterials is an important problem because of numerous potential applications in far-field subwavelength imaging [16], enhanced nonlinearities [17], nanoscale wave guiding, and strong light confinement [18]. Some realizations of tunable THz metamaterials were presented, for example, in Refs. [19,20]. The majority of them represent an array of resonators whose capacity and/or inductivity is changed by external influences [19].

Here we propose a new concept of an ultrahomogeneous temperature tunable metamaterial based on a semiconductor superlattice for THz applications. Here, the term *ultrahomogeneous* implies that the superlattice consists of coupled quantum wells separated by thin ($\sim$1 nm) tunnel-transparent barriers. Superlattices with layers of such a thickness are possible to fabricate with various semiconductor materials, for example, GaInAs/AlInAs [21], GaAs/AlGaAs [22], GaSb/AlGaSb [23], and Si/GeSi [24]. Particularly, such structures are used in quantum cascade lasers [21].

In the case of a superlattice with thin barriers, in contrast to thick ones considered, e.g., in Refs. [25,26], electron wave functions are spread over many periods of the structure because of the tunnel transparency of the barriers. Hence, quantum effects are particularly relevant and, therefore, it is incorrect to describe the dielectric function of each layer separately and then apply the homogenization procedure. Therefore, another approach, which takes into account the wave functions of the carriers, their energy spectrum modified by the superlattice potential and the carrier distribution function, should be used. The proper approximation (quantum homogenization) is discussed in the next section.

It has been shown that highly doped semiconductor superlattices can exhibit properties of a hyperbolic medium at infrared frequencies [26–29]. The frequency range of the hyperbolic regime is defined by plasma frequency, which depends on the free carrier concentration. Free carrier concentration in semiconductors is extremely sensitive to the temperature, in contrast to dielectrics and metals. For example, in the vicinity of the donor activation temperature, it can change by several orders [30]. We have shown that high temperature sensitivity of plasma frequency in a semiconductor metamaterial can be exploited for the efficient tuning of the metamaterial's optical properties in the THz region and stimulation of the topological transition from the dielectric to hyperbolic regime.

The paper is organized as follows. In Sec. II we develop a quantum homogenization theory and derive the main equations

*ki.koshelev@gmail.com
†bogdanov@ioffe.mail.ru

for the effective permittivity tensor. In Secs. III and IV, we analyze the band structure and effective dielectric function of a Te-doped GaAs/$Al_{0.3}Ga_{0.7}As$ superlattice depending on the temperature and frequency of the electromagnetic field. In Sec. V, numerical simulation of an experiment on the measurement of the reflectance spectrum from the superlattice slab is performed. In Sec. VI we discuss a figure of merit and tunability of semiconductor metamaterials. Finally, in Sec. VII we summarize our major results.

II. MODEL

A. Quantum homogenization

The homogenization problem has a long history [31,32] but it is still being discussed today [33–36]. Here we extend the classical homogenization theory of multilayer structures to the case of tunnel transparent layers.

Within the effective medium approximation, a multilayered structure with layer permittivities ε_i and layer thicknesses d_i can be considered as a uniaxial optical crystal with permittivity tensor (1) whose principle components are determined as

$$\frac{1}{\varepsilon_\parallel}=\frac{1}{d}\sum_i\frac{d_i}{\varepsilon_i},\quad \varepsilon_\perp=\frac{1}{d}\sum_i d_i\varepsilon_i,\quad d=\sum_i d_i. \tag{2}$$

As we have mentioned in the Introduction, these formulas are inapplicable when the thickness of the layers is comparable with electron wavelength and, therefore, quantum mechanics laws become relevant. We consider a more accurate approach based on the Kubo formula [37]. It takes into account the distribution function of the carriers, their wave functions, and spectrum modified by the superlattice potential:

$$\varepsilon_\alpha(\omega)=\varepsilon_\alpha^\infty\left(1-\frac{\Omega_\alpha^2}{\omega(\omega+i\gamma)}\right)+\frac{4\pi i}{\omega}\sigma_\alpha(\omega). \tag{3}$$

Here and in what follows, the index $\alpha=\parallel,\perp$ corresponds to the directions along and across the optical axis of the metamaterial. Parameter $\varepsilon_\alpha^\infty$ is a permittivity of the lattice without free carriers, and γ is the inverse momentum relaxation time of the carriers which is supposed to be isotropic for simplicity.

The first term interprets the classical Drude-Lorentz formula. One can see that implementation of a superlattice in a semiconductor makes its plasma frequency anisotropic and we can distinguish plasma frequencies along ($\Omega_\parallel$) and across ($\Omega_\perp$) the optical axis:

$$\Omega_\alpha^2=\frac{4\pi e^2}{\varepsilon^\infty}\frac{2}{(2\pi\hbar)^3}\sum_i\iiint f(E,\mu,T)\frac{\partial^2E_i}{\partial p_\alpha^2}d^3p. \tag{4}$$

Here E_i is the carrier energy in the ith miniband which depends on the momentum $\mathbf{p}$, $f(E,\mu,T)$ is the Fermi-Dirac distribution function, μ is the chemical potential, and T is the temperature. The sum is over all the minibands. Here we neglect hole contribution into the plasma frequency because we will consider n-doped semiconductor structures. Equation (4) is similar to the classical definition of plasma frequency:

$$\Omega^2=\frac{4\pi ne^2}{\varepsilon^\infty m^*}. \tag{5}$$

Indeed, the difference between Eq. (4) and Eq. (5) is that in Eq. (4) we just average the inverse effective anisotropic mass $1/m^*_{\perp,\parallel}=\partial^2E/\partial p^2_{\perp,\parallel}$ with distribution function $f(E,\mu,T)$.

The second term in Eq. (3) describes interband transitions:

$$\sigma_\alpha=\frac{2i}{(2\pi\hbar)^3}\sum_{i,j}\iiint\frac{f(E_i)-f(E_j)}{\omega_{ij}-\omega+i\gamma}\frac{\left|\hat J_\alpha^{ij}\right|^2}{\hbar\omega_{ji}}d^3p. \tag{6}$$

Here $\hat J_\alpha^{ij}=\langle i,\mathbf{p}|\,\hat J_\alpha\,|j,\mathbf{p}\rangle$ is the matrix element of the current operator $\hat J_\alpha$ between the unperturbed eigenstates of the superlattice and $\hbar\omega_{ij}=E_i-E_j$.

In order to calculate $\Omega_\perp$ and $\Omega_\parallel$ we need to determine the energy spectrum $E_i(\mathbf{p})$ and the chemical potential μ.

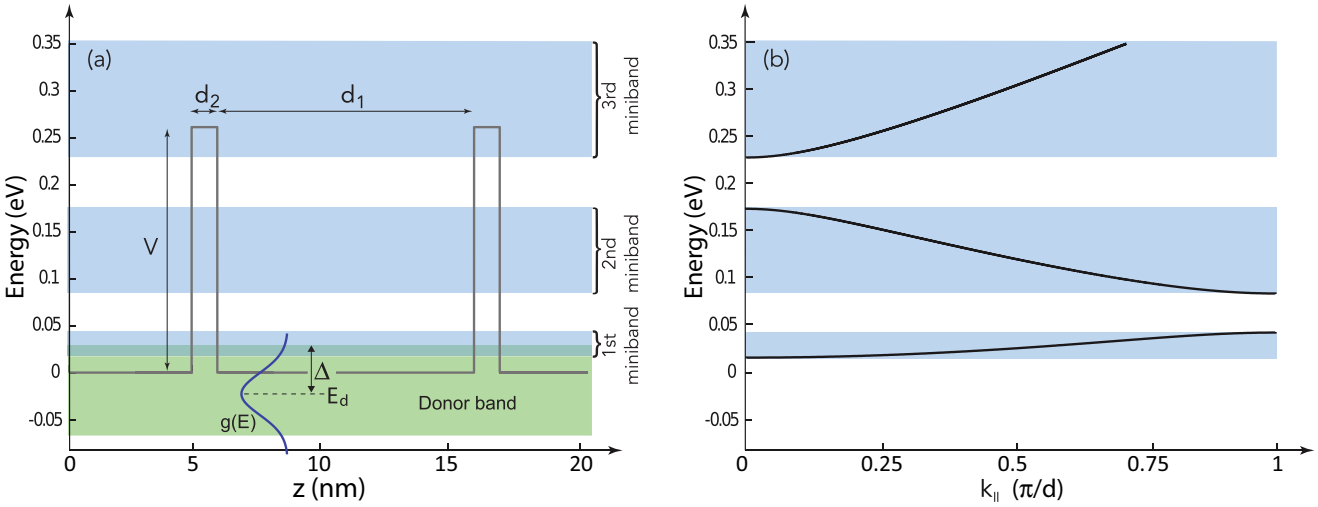

FIG. 1. (Color online) (a) Conduction band profile of the n-doped superlattice. Blue shaded areas represent the energy of the minibands. The green shaded area corresponds to the donor band. Thicknesses of the well and the barrier are denoted as d_1 and d_2, respectively; V is the height of the barrier; and $g(E)$ is a donor distribution function with standard deviation Δ and a maximum at E_d. (b) Electron energy dispersion in the GaAs/$Al_{0.3}Ga_{0.7}As$ superlattice with the following parameters: $d_1=10$ nm, $d_2=1$ nm, $V=0.26$ eV.

B. Energy spectrum of carriers

Let us consider a periodic semiconductor superlattice with period d consisting of a quantum well with thickness d_1 and a barrier with thickness d_2 and height V [Fig. 1(a)]. Effective masses in the well and barrier we put equal to m_1 and m_2, respectively.

The total energy of an electron in a superlattice can be represented as the sum of two terms which correspond to electron motion across and along the optical axis:

$$E_i(\mathbf{p}) = \frac{p_\perp^2}{2m_\perp^*} + E_i(p_\parallel). \tag{7}$$

Here $m_\perp^*$ is the effective mass of electrons in the direction across the optical axis. We take it equal to the effective electron mass in a bulk material. The second term of the right-hand side describes energy dispersion of electrons in the ith miniband. It can be found from the dispersion equation

$$\cos(p_\parallel d/\hbar) = \cos(p_1 d_1/\hbar)\cos(p_2 d_2/\hbar) - \frac{1}{2}\sin(p_1 d_1/\hbar) \times \sin(p_2 d_2/\hbar)\left(\frac{p_1 m_2}{p_2 m_1} + \frac{p_2 m_1}{p_1 m_2}\right), \tag{8}$$

where $p_1 = \sqrt{2m_1 E(p_\parallel)}$, $p_2 = \sqrt{2m_2[E(p_\parallel) - V]}$. This dispersion equation can be obtained from the Schrödinger equation using Floquet's theorem.

C. Chemical potential

Efficient temperature manipulation of free carrier concentration can be realized in narrow-gap or in doped semiconductor structures. Temperature tuning in metamaterials based on narrow-gap semiconductors was partially analyzed in Ref. [38]. Here we consider the case of doped semiconductor structures on the example of a superlattice with quantum wells uniformly doped with shallow donors.

In highly doped structures, wave functions of neighbor donors can overlap. This results in a shift of donor levels and formation of a donor band. In the case of a considerable shift, the donor band can overlap with the conduction band. This phenomenon is called the Mott transition and will be discussed further.

The chemical potential μ can be calculated from the electroneutrality condition [30]. It states that free carrier concentration is equal to the concentration of ionized donors:

$$\sum_i \int f(\mathbf{p},\mu,T)\frac{2d^3p}{(2\pi\hbar)^3} = n_d \int \frac{g(E)dE}{2e^{(\mu-E)/(kT)}+1}. \tag{9}$$

Here n_d is the full donor concentration, and $g(E)$ is a donor distribution function which can be approximated by a Gaussian [39] with standard deviation Δ and maximum at E_d [40].

III. BAND STRUCTURE OF THE SUPERLATTICE

The model described above is applicable for superlattices of various compounds and designs. As an example, let us consider a superlattice that consists of GaAs quantum wells and $Al_{0.3}Ga_{0.7}As$ barriers. Thickness of the quantum well d_1 and the barrier d_2 we put equal to 10 and 1 nm, respectively. We consider the high frequency permittivity in Eq. (3) to be isotropic ($\varepsilon_\parallel^\infty = \varepsilon_\perp^\infty$) and put it equal to 11 [41]. In-plane electron effective mass $m_\perp^*$ we put equal to 0.067 times the free-electron mass. The calculated band structure and electron dispersion are shown in Fig. 1(b). We consider that quantum wells are uniformly doped with Te donors with concentration $n_d = 1\times10^{18}$ cm^{-3}. The energies of Te donors in bulk GaAs and in the superlattice are slightly different due to quantum confinement that arises from the superlattice potential. We neglect this difference and put $E_d = 0.03$ eV as in a bulk material [30]. The standard deviation of the donor distribution function Δ for such a doping level is about several hundredths of an electron volt. In the structure under consideration we put $\Delta = 0.03$ eV, which is in accordance with Refs. [40,42].

The width of the first miniband is about several hundredths of an electron volt, which is comparable with the gap between the minibands. So, both weak-coupling and tight-binding approximations are poorly applicable for the structure under consideration.

For the chosen parameters, the overlap of donor miniband and first miniband is approximately equal to 0.01 eV. This means that even at zero temperature there are free carriers in the conduction band and their Fermi energy is about 0.01 eV. This corresponds to a concentration of about 10^{16} cm^{-3}. A simple estimation of plasma frequency using Eq. (5) yields $\Omega/(2\pi) \sim 1$ THz.

IV. EFFECTIVE DIELECTRIC FUNCTION OF THE SUPERLATTICE

We calculate the frequency and temperature dependencies of the permittivity tensor components using the quantum homogenization approach [Eq. (4)]. The frequency dependence of $\varepsilon_\perp$ and $\varepsilon_\parallel$ at room temperature is shown in Fig. 2(a). The average energy between minibands and, therefore, frequencies of interband transitions are about 0.05 eV [Fig. 1(a)], which corresponds to a frequency of 10 THz. So, the contribution of interband transition into the dielectric function [second term in Eq. (3)] can be neglected at frequencies of 1 THz without any considerable precision losses. Thus, quantum homogenization predicts that, beyond the interband transition, the tensor components of a superlattice with thin layers can be described within the classical Drude-Lorentz formula with plasma frequency described by Eq. (4).

These results qualitatively differ from effective parameters obtained within the classical homogenization procedure which predicts a resonance behavior of $\varepsilon_\parallel$ at a nonzero frequency. There is no contradiction here. Classical homogenization implies that all layers are isolated from each other and that the carriers do not move from one layer into a neighboring one. Qualitatively it is equivalent to the restoring force that obstructs the carrier transport. This force results in an appearance of the resonance in $\varepsilon_\parallel$. Quantum homogenization implies that the barriers are tunnel transparent and charges can move freely throughout the whole volume of the sample. Therefore, the dielectric function $\varepsilon_\parallel$ is similar to that of a metal but takes into account interband transitions.

Homogenization theory developed here is applicable when the barriers are tunnel transparent. Condition of tunnel transparency and, therefore, application limit can be roughly

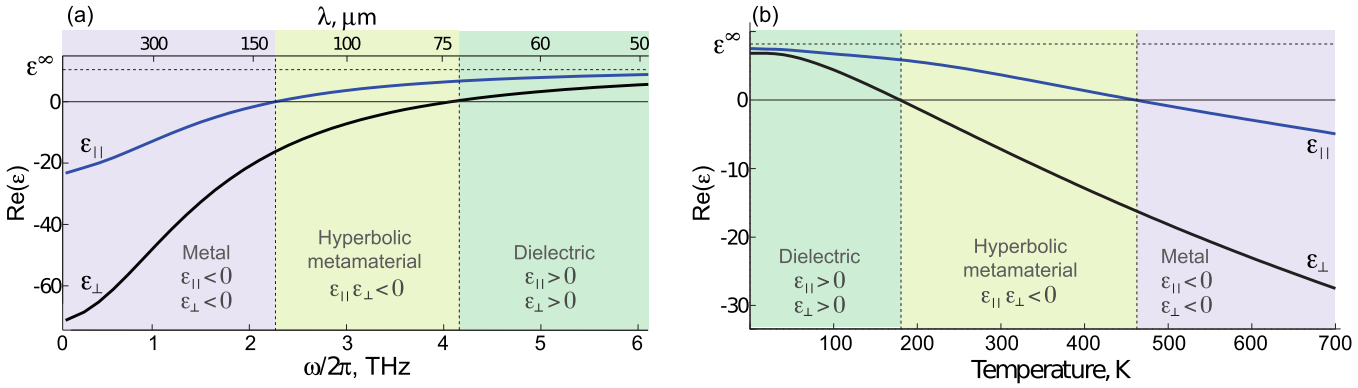

FIG. 2. (Color online) (a) Frequency dependence of the real part of the dielectric function along (blue line) and across (black line) the optical axis. Temperature $T = 300$ K. (b) Temperature dependence of the real part of the dielectric function along (blue line) and across (black line) the optical axis. Permittivity of the media without free carriers ε^{∞} is shown by the dashed line. Frequency $\omega/2\pi = 3$ THz.

estimated as

$$d_2 < \left(\frac{\hbar^2}{2m_{\perp}^* V}\right)^{1/2}. \tag{10}$$

This condition means that barrier thickness d_2 should be less than the penetration depth of the electron wave function into the barrier. For the structure under consideration, Eq. (10) yields $d_2 \lesssim 2$ nm. For narrow-band semiconductors (e.g., InAs or InSb) with barrier height $V \sim 0.1$ eV Eq. (10) yields $d_2 \lesssim 5$ nm.

One can see from Fig. 2(a) that there are three frequency regions which correspond to different forms of the equal-frequency surfaces in k space: (i) at frequencies $\omega/2\pi > 4.1$ THz the material behaves like a dielectric; (ii) at frequencies 2.2 THz $< \omega/2\pi < 4.1$ THz the form of the equal-frequency surface is a hyperboloid and the material exhibits optical properties of HMM; (iii) at $\omega/2\pi < 2.2$ THz electromagnetic waves decay exponentially into the medium, similar to the behavior in a metal.

The temperature dependence of $\varepsilon_{\perp}$ and $\varepsilon_{\parallel}$ at a frequency of 3 THz is shown in Fig. 2(b). One can see that the material behaves as a dielectric, HMM, or a metal depending on the temperature. Dielectric dispersion can be realized at the temperature of liquid nitrogen; the hyperbolic regime is achieved at room temperature. Thus, a topological transition for THz radiation can be realized at temperatures reasonable for an experiment.

The temperature dependence of the permittivity tensor components is weak at low temperatures. This is explained by the fact that the main parts of the donor levels are noticeably separated from the conduction band bottom, thus the activation of electrons on such levels occurs at temperature $kT \sim E_d$. At higher temperatures when all donors are ionized, the dielectric functions $\varepsilon_{\perp}$ and $\varepsilon_{\parallel}$ tend to constant values. In our case it occurs at temperatures much higher than the melting point of GaAs which is 1511 K [41].

Figure 3 represents a topological phase state diagram. Solid lines show the temperature dependence of the longitudinal $\Omega_{\parallel}$ and transversal $\Omega_{\perp}$ plasma frequencies. These lines divide the plane of the figure into three regions. It follows from Eq. (3) that every region corresponds to one of the possible regimes: dielectric, metal, or hyperbolic. The shapes of equal-frequency surfaces corresponding to each regime are shown in the insets of Fig. 3.

One can see that plasma frequencies $\Omega_{\parallel}$ and $\Omega_{\perp}$ are not equal to zero at low temperatures. This is explained by the overlapping of the donor and first minibands, the so-called Mott transition [43]. A part of the carriers does not freeze-out at low temperatures and makes a contribution into the plasma frequencies.

V. SIMULATION OF EXPERIMENT

The efficiency of temperature tuning and the presence of a topological transition in a metamaterial based on a semiconductor superlattice can be confirmed experimentally by the measurement of a reflectance spectrum from the metamaterial. Here we provide a numerical simulation of a possible experiment. Calculations of the reflectance spectrum were performed by using a transfer matrix technique and the Fresnel equations for the interface between uniaxial and isotropic materials.

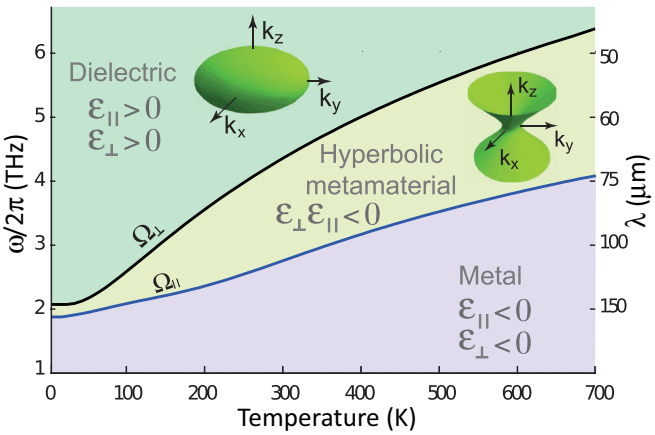

FIG. 3. (Color online) Temperature dependence of plasma frequency along the optical axis (blue line) and across the optical axis (black line). Insets show the shape of equal-frequency surfaces in the dielectric and hyperbolic regimes.

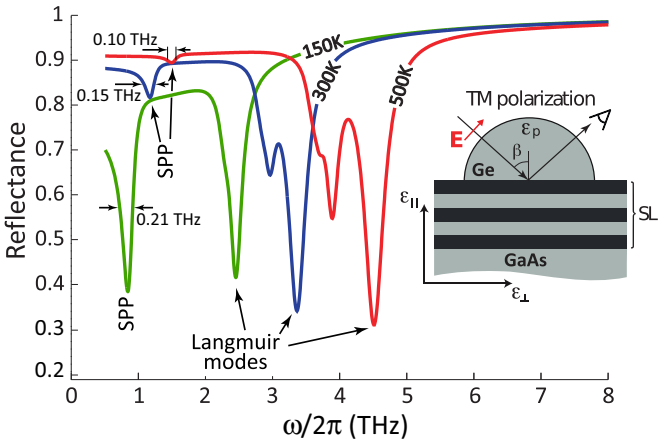

FIG. 4. (Color online) Frequency dependence of reflectance at three different temperatures. The inset shows the relative orientation of the dielectric function ($\varepsilon_\perp$ and $\varepsilon_\parallel$), the electric-field vector (transverse magnetic), the layered structure, and a spherical prism with permittivity $\varepsilon_p = 16$. Angle of incidence is $\beta = 60^\circ$.

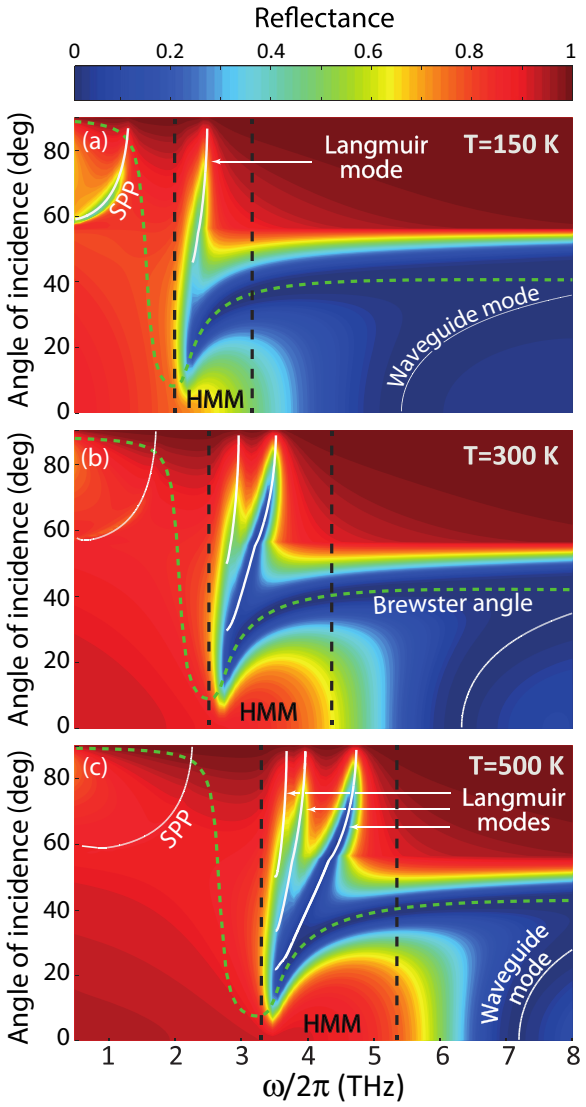

FIG. 5. (Color online) Simulation of reflectance spectrum from a 10 μm GaAs/$Al_{0.3}Ga_{0.7}As$ superlattice for different incident angles β. Incident wave has TM polarization. Parameters of the superlattice are mentioned in Sec. III. Temperature takes values equal to 150, 300, and 500 K. Inverse momentum relaxation time is $\gamma = 1 \times 10^{12}$ s^{-1}. The green dashed line corresponds to the Brewster's angle which is determined by Eq. (11). White solid lines show the dispersion of waveguide modes. The frequency interval between black dashed lines corresponds to the hyperbolic regime of metamaterial.

The scheme of the experiment is shown in the inset of Fig. 4. A plane electromagnetic wave of TM polarization is supposed to be incident at the angle β on the 10 μm GaAs/$Al_{0.3}Ga_{0.7}As$ superlattice grown on an undoped GaAs substrate. The inverse momentum relaxation time of electrons in the superlattice γ [see Eq. (3)] we put equal to 1×10^{12} s^{-1}. For the sake of simplicity, we neglect the temperature dependence of γ. In order to get efficient excitation of the optical states with high wave vectors we suppose that the wave incident on the sample passes through an undoped Ge spherical prism with permittivity $\varepsilon_p = 16$.

The frequency dependence of the reflectance for different temperatures at fixed angle of incidence $\beta = 60^\circ$ is shown in Fig. 4. Each curve has several minima corresponding to excitation of eigenmodes of the slab. Minimum at low frequency corresponds to excitation of surface plasmon polariton (SPP) when the superlattice exhibits properties of a metal. One can see that SPP excitation becomes weaker with temperature and it is nearly lacking at 500 K. Such a behavior is explained by the nonresonant nature of SPP excitation in the proposed geometry (see inset in Fig. 4) in contrast to the geometries analyzed in Ref. [44] where excitation is resonant. Increasing of temperature results in increasing of SPP resonance quality [45] and weakening of the coupling between incident wave and SPP.

The minima at higher frequencies correspond to the excitation of multiple Langmuir modes (bulk plasmons) intrinsic to hyperbolic metamaterials [4,46,47]. One can see that resonances corresponding to the Langmuir modes are highly tunable with temperature. For example, main resonance shows blueshift about 2 THz as temperature increases from 150 to 500 K. The same temperature increasing results in increasing of the reflection coefficient from 0.4 to 0.9.

A more full and illustrative picture can be obtained by measuring of the reflection coefficient map—its dependence on both incident angle β and frequency ω (Fig. 5). A comparison of the reflection coefficient map with the numerically calculated dispersion of eigenmodes (white lines in Fig. 5) confirms excitation of SPP in the metallic regime, Langmuir modes in the hyperbolic, and waveguide mode in the dielectric. The boundary of the hyperbolic regime can be determined from the reflection coefficient map. The lower boundary corresponds to the frequency cutoff of the Langmuir modes and the upper boundary corresponds to the drastic change of reflection coefficient at normal incidence. In the dielectric regime, at angles less than the critical angle, weak excitation of the waveguide mode is observed.

The boundaries are shown in Fig. 5 by black dashed lines. Boundary positions are in a good agreement with results shown

in Fig. 3. Increasing loss γ results in smearing of the hyperbolic regime boundaries.

One can see that the frequency range of the hyperbolic regime exhibits blueshift and becomes wider. So, increasing the temperature from 150 to 300 K results in blueshift of the lower and upper boundaries of the hyperbolic regime from 2.0 and 3 THz [Fig. 5(a)] to 3.2 and 5.8 THz [Fig. 5(c)]. If the frequency range of the hyperbolic regime is wide enough, several Langmuir modes can be distinguished in the reflectance spectrum.

Another minimum in the reflectance spectrum appearing in the hyperbolic and dielectric regimes is related to the Brewster angle α_B as we consider TM-polarized incident wave. For an anisotropic uniaxial crystal α_B can be determined as [48]

$$\alpha_B = \mathrm{Re}\left\{\arcsin\left(\sqrt{\frac{\varepsilon_\perp\varepsilon_\parallel - \varepsilon_\parallel\varepsilon_p}{\varepsilon_\perp\varepsilon_\parallel - \varepsilon_p^2}}\right)\right\}. \quad (11)$$

The frequency dependence of α_B is shown in Fig. 5 by a green dashed line.

VI. LOSSES

One significant stumbling block of HMMs limiting their functionality and preventing their applications is intrinsic loss. The main loss mechanisms in semiconductors are free carrier absorption, fundamental absorption, and absorption due to optical phonons [30]. Fundamental absorption is dominant in the optical range. Absorption due to optical phonons occurs in polar semiconductors and has resonance behavior around wavelengths 30–35 μm. Free carrier absorption increases with wavelength as square of the wavelength [49,50], so this loss makes the main contribution in the THz spectral range.

In the previous section we have shown that the superlattice plays the role of a waveguide supporting SPP, waveguide, or Langmuir modes depending on the regime of a metamaterial. The figure of merit (FOM) of the metamaterial slab can be introduced as

$$\eta(\omega) = \frac{\mathrm{Re}(k_z)}{\mathrm{Im}(k_z)}. \quad (12)$$

Here k_z is a frequency dependent propagation constant unique for each eigenmode. However, it is possible to show from the Maxwell's equations that η has a weak dependence on the mode number in the hyperbolic regime. For this reason, we plotted η in Fig. 6 only for the dominant Langmuir mode. An analytical expression for η can be derived with the perturbation theory using γ/ω as a small parameter:

$$\eta = \frac{2\omega}{\gamma\varepsilon^\infty}\frac{\varepsilon_\perp\varepsilon_\parallel}{\varepsilon_\perp - \varepsilon_\parallel}. \quad (13)$$

A plot of this equation for different temperatures is shown in Fig. 6 by circles. Equation (13) yields right position of FOM maximum which is around

$$\omega_0 = \left(\frac{\Omega_\parallel^2 + \Omega_\perp^2}{2}\right)^{1/2}. \quad (14)$$

However, the maximum value of η obtained from Eq. (13) is a little bit exaggerated.

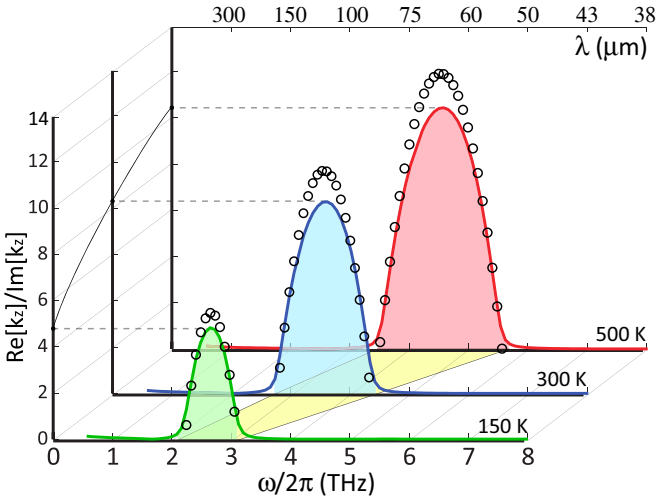

FIG. 6. (Color online) Frequency dependence of FOM [$\eta = \mathrm{Re}(k_z)/\mathrm{Im}(k_z)$] for the main Langmuir mode at temperatures 150, 300, and 500 K. Analytical approximation given by Eq. (13) is shown by circles.

As was shown in the previous section (see Fig. 5), the reflectance spectrum is the most sensitive to the temperature and, hence, can be efficiently tuned, in the hyperbolic regime (at the frequencies of several THz in our case). Combination of FOM's maximum and high tunability make proposed metamaterial very promising for THz applications.

A shift of the optimal operation frequency toward the optical range is possible by increasing the doping level. For example, a simple estimation using Eq. (5) yields the value of plasma frequency $\Omega_p/2\pi \sim 1 \times 10^{14}$ Hz for free carrier concentration 1×10^{20} cm^{-3}, effective mass $m^* \sim 0.1m_e$, and permittivity $\varepsilon^\infty \sim 10$. It corresponds to the wavelength $\lambda_p \sim 3$ μm. However, screening and strong random potential in highly doped semiconductors [30,43] embarrass tunability characteristics of metamaterial.

VII. CONCLUSION

In this work we proposed a new concept of an ultra-homogeneous temperature-tunable metamaterial based on a doped semiconductor superlattice. We have shown that the classical homogenization procedure is inapplicable for the description of the metamaterial in terms of effective parameters because of the tunnel transparency of the barriers separating the quantum wells and that quantum homogenization should be used. We developed the theory of quantum homogenization applied to semiconductor nanostructured metamaterials. It is based on the Kubo formula for conductivity and takes into account wave functions of the carriers, their energy spectrum, and distribution function. The main limitation of quantum homogenization theory is associated with tunnel transparency of barriers. The barrier thickness should be less than the penetration depth of the electron wave function into the barriers. Simple estimation shows that, for example, the quantum homogenization theory is applicable for structures with barrier height 0.2 eV if their thickness is less than 2

nm (for wide-gap semiconductors) and 5 nm (for narrow-gap semiconductors).

We have shown that the components of the dielectric tensor of the semiconductor metamaterial can be efficiently manipulated by external temperature. Efficient temperature tunability is a distinctive feature of semiconductors which is explained by the high sensitivity of free carrier concentration to the temperature. On the example of a $GaAs/Al_{0.3}Ga_{0.7}As$ semiconductor superlattice with Te-doped quantum wells ($n_d = 1 \times 10^{18}$ cm^{-3}) we have shown that the temperature of the topological transition from the dielectric to hyperbolic regime $\sim$300 K for the frequency $\sim$4 THz. Numerical simulation shows that the topological transition can be detected in an experiment on the measurement of reflectance spectrum from the superlattice slab.

A significant advantage of semiconductor metamaterials is the possibility of their direct integration into optolectronic devices and optical integrated circuits. Moreover, semiconductor materials combine two important features. On one hand, the energy spectrum of the carriers in semiconductor nanostructures can be precisely tailored with quantum engineering technologies. On the other hand, there are many methods of dynamic control of the electron distribution function in semiconductors, which are well developed and widely applied in nano- and optoelectronics. These are, for example, electrical injection, optical pumping, thermal excitation, electron heating by electric field, etc. The advantages mentioned earlier and the rich functionality of semiconductor metamaterials allow one to consider them as an important element of future optoelectronics.

ACKNOWLEDGMENTS

This work was partially supported by the Government of the Russian Federation (Grant No. 074-U01), by the Russian Foundation for Basic Research (14-02-01223, 13-02-00411) by FP7 (PIRSES-612564), and the Federal Program on Support of Leading Scientific Schools (NSh-5062.2014.2). All numerical simulations were supported by the Russian Science Foundation (Project No. 15-12-20028).

[1] D. R. Smith and D. Schurig, Phys. Rev. Lett. **90**, 077405 (2003).
[2] Y. Guo, W. Newman, C. L. Cortes, and Z. Jacob, Adv. Optoelectron. **2012**, 1 (2012).
[3] C. Cortes, W. Newman, S. Molesky, and Z. Jacob, J. Optics **14**, 063001 (2012).
[4] M. Noginov, M. Lapine, V. Podolskiy, and Y. Kivshar, Opt. Express **21**, 14895 (2013).
[5] A. Poddubny, I. Iorsh, P. Belov, and Y. Kivshar, Nat. Photonics **7**, 948 (2013).
[6] L. Ferrari, C. Wu, D. Lepage, X. Zhang, and Z. Liu, Prog. Quantum Electron. **40**, 1 (2015).
[7] Z. Jacob, I. I. Smolyaninov, and E. E. Narimanov, Appl. Phys. Lett. **100**, 181105 (2012).
[8] A. D. Boardman, V. V. Grimalsky, Y. S. Kivshar, S. V. Koshevaya, M. Lapine, N. M. Litchinitser, V. N. Malnev, M. Noginov, Y. G. Rapoport, and V. M. Shalaev, Laser Photonics Rev. **5**, 287 (2011).
[9] I. I. Smolyaninov and E. E. Narimanov, Phys. Rev. Lett. **105**, 067402 (2010).
[10] J.-Y. Ou, E. Plum, L. Jiang, and N. I. Zheludev, Nano Lett. **11**, 2142 (2011).
[11] J. Zhu, J. Han, Z. Tian, J. Gu, Z. Chen, and W. Zhang, Opt. Commun. **284**, 3129 (2011).
[12] S. H. Lee, M. Choi, T.-T. Kim, S. Lee, M. Liu, X. Yin, H. K. Choi, S. S. Lee, C.-G. Choi, S.-Y. Choi, X. Zhang, and B. Min, Nat. Mater. **11**, 936 (2012).
[13] H. N. Krishnamoorthy, Z. Jacob, E. Narimanov, I. Kretzschmar, and V. M. Menon, Science **336**, 205 (2012).
[14] O. Y. Yermakov, A. I. Ovcharenko, M. Song, A. A. Bogdanov, I. V. Iorsh, and Y. S. Kivshar, Phys. Rev. B **91**, 235423 (2015).
[15] I. I. Smolyaninov, J. Phys.: Condens. Matter **26**, 305701 (2014).
[16] Z. Jacob, L. V. Alekseyev, and E. Narimanov, Opt. Express **14**, 8247 (2006).
[17] G. A. Wurtz, R. Pollard, W. Hendren, G. Wiederrecht, D. Gosztola, V. Podolskiy, and A. V. Zayats, Nat. Nanotechnol. **6**, 107 (2011).
[18] A. A. Govyadinov and V. A. Podolskiy, Phys. Rev. B **73**, 155108 (2006).
[19] H. Tao, A. C. Strikwerda, K. Fan, W. J. Padilla, X. Zhang, and R. D. Averitt, J. Infrared, Millimeter, Terahertz Waves **32**, 580 (2011).
[20] J. Yao, X. Yang, X. Yin, G. Bartal, and X. Zhang, Proc. Natl. Acad. Sci. USA **108**, 11327 (2011).
[21] C. Gmachl, F. Capasso, D. L. Sivco, and A. Y. Cho, Rep. Prog. Phys. **64**, 1533 (2001).
[22] R. Dingle, A. Gossard, and W. Wiegmann, Phys. Rev. Lett. **34**, 1327 (1975).
[23] A. Herrmann, T. Lehnhardt, M. Strauß, M. Kamp, and A. Forchel, Surf. Interface Anal. **43**, 673 (2011).
[24] S. Golod, V. Y. Prinz, V. Mashanov, and A. Gutakovsky, Semiconductor Sci. Technol. **16**, 181 (2001).
[25] J. R. Plumridge, R. J. Steed, and C. C. Phillips, Phys. Rev. B **77**, 205428 (2008).
[26] P. Shekhar and Z. Jacob, Phys. Rev. B **90**, 045313 (2014).
[27] K. Y. Yang, V. Giannini, A. O. Bak, H. Amrania, S. A. Maier, and C. C. Phillips, Phys. Rev. B **86**, 075309 (2012).
[28] G. V. Naik, J. Liu, A. V. Kildishev, V. M. Shalaev, and A. Boltasseva, Proc. Natl. Acad. Sci. USA **109**, 8834 (2012).
[29] A. J. Hoffman, L. Alekseyev, S. S. Howard, K. J. Franz, D. Wasserman, V. A. Podolskiy, E. E. Narimanov, D. L. Sivco, and C. Gmachl, Nat. Mater. **6**, 946 (2007).
[30] S. M. Sze and K. K. Ng, *Physics of Semiconductor Devices* (Wiley, New York, 2006).
[31] J. M. Garnett, Philos. Trans. R. Soc. London, Ser. A **205**, 237 (1906).
[32] V. D. Bruggeman, Ann. Phys. **416**, 665 (1935).
[33] C. R. Simovski, J. Optics **13**, 013001 (2011).
[34] M. G. Silveirinha, Phys. Rev. B **75**, 115104 (2007).
[35] M. G. Silveirinha and C. A. Fernandes, IEEE Trans. Microwave Theory Tech. **53**, 1418 (2005).

[36] T. D. Myles, A. A. Peracchio, and W. K. Chiu, J. Appl. Phys. **117**, 025101 (2015).
[37] Y. Murayama, *Mesoscopic Systems: Fundamentals and Applications* (Wiley, New York, 2008).
[38] S. T. Bui, V. D. Nguyen, X. K. Bui, T. T. Nguyen, P. Lievens, Y. Lee, and D. L. Vu, J. Opt. **15**, 075101 (2013).
[39] For the sake of simplicity, we neglect the effects of the Coulomb gap [43, 51].
[40] T. Brody, J. Appl. Phys. **33**, 100 (1962).
[41] S. Adachi, *GaAs and Related Materials* (World Scientific, Singapore, 1994).
[42] E. M. Conwell, Phys. Rev. **103**, 51 (1956).
[43] B. I. Shklovskii and A. L. Efros, *Electronic Properties of Doped Semiconductors* (Springer-Verlag, Berlin, 1984).
[44] S. A. Maier, *Plasmonics: Fundamentals and Applications* (Springer Science+Business Media LLC, New York, 2007).
[45] Quality factor of SPP resonance can be estimated as the ratio of an average plasma frequency to inverse momentum relaxation time of carriers γ.
[46] A. A. Bogdanov and R. A. Suris, Phys. Rev. B **83**, 125316 (2011).
[47] A. A. Bogdanov and R. A. Suris, JETP Lett. **96**, 49 (2012).
[48] W. Shu, Z. Ren, H. Luo, and F. Li, Appl. Phys. A **87**, 297 (2007).
[49] P. Y. Yu, M. Cardona, and L. J. Sham, Physics Today **50** (11), 76 (1997).
[50] A. Bogdanov and R. Suris, Physica Status Solidi B **249**, 885 (2012).
[51] A. Efros and B. Shklovskii, J. Phys. C **8**, L49 (1975).